Solar Phys
DOI 10.1007/s11207-013-0293-9

Comparison of Cone Model Parameters for Halo Coronal Mass Ejections

Hyeonock Na · Y.-J. Moon · Soojeong Jang · Kyoung-Sun Lee · Hae-Yeon Kim

Received: 19 December 2011 / Accepted: 1 April 2013

Abstract Halo coronal mass ejections (HCMEs) are a major cause of geomagnetic storms, hence their three-dimensional structures are important for space weather. We compare three cone models: an elliptical-cone model, an ice-cream-cone model, and an asymmetric-cone model. These models allow us to determine three-dimensional parameters of HCMEs such as radial speed, angular width, and the angle [γ] between sky plane and cone axis. We compare these parameters obtained from three models using 62 HCMEs observed by SOHO/LASCO from 2001 to 2002. Then we obtain the root-mean-square (RMS) error between the highest measured projection speeds and their calculated projection speeds from the cone models. As a result, we find that the radial speeds obtained from the models are well correlated with one another ($R > 0.8$). The correlation coefficients between angular widths range from 0.1 to 0.48 and those between γ-values range from −0.08 to 0.47, which is much smaller than expected. The reason may be the different assumptions and methods. The RMS errors between the highest measured projection speeds and the highest estimated projection speeds of the elliptical-cone model, the ice-cream-cone model, and the asymmetric-cone model are 376 $\mathrm{km\,s^{-1}}$, 169 $\mathrm{km\,s^{-1}}$, and 152 $\mathrm{km\,s^{-1}}$. We obtain the correlation coefficients between the location from the models and the flare location ($R > 0.45$). Finally, we discuss strengths and weaknesses of these models in terms of space-weather application.

Keywords Coronal mass ejections, initiation and propagation

H. Na · Y.-J. Moon (✉) · S. Jang
School of Space Research, Kyung Hee University, Yongin, Korea
e-mail: moonyj@khu.ac.kr

H. Na
e-mail: nho0512@khu.ac.kr

K.-S. Lee
Astronomy Program, Department of Physics and Astronomy, Seoul National University, Seoul, Korea

H.-Y. Kim
National Meteorological Satellite Center, Korea Meteorological Administration, Jincheon, Korea

Published online: 07 May 2013

1. Introduction

Coronal mass ejections (CMEs) are magnetized plasma ejected from the Sun. CMEs whose bright clouds surround the entire Sun are called halo coronal mass ejections (HCMEs), which were first reported by Howard *et al.* (1982). The HCMEs propagating toward (or away from) the Earth are called frontside (backside) ones. The frontside HCMEs are accepted as the main cause of geomagnetic storms (Gosling *et al.*, 1991; Brueckner *et al.*, 1998; Cane, Richardson, and St. Cyr, 2000; Gopalswamy *et al.*, 2000; Webb *et al.*, 2000; Wang *et al.*, 2002). Therefore, determining the kinematic and geometric parameters of HCMEs such as the radial velocity, angular width, and source location is important for space-weather forecasting (Taktakishvili *et al.*, 2009; Falkenberg *et al.*, 2010; Taktakishvili, MacNeice, and Odstrcil, 2010).

The HCMEs have been mainly observed by single-spacecraft coronagraph observation such as the *Large Angle Spectroscopic Coronagraph* (LASCO: Brueckner *et al.*, 1995) onboard the *Solar and Heliospheric Observatory* (SOHO). Single-spacecraft coronagraph observations are subject to projection effects. From this we can only identify the information about HCMEs projected on the plane of the sky: an apparent angular width and an apparent speed. In the coronagraph images, the CMEs near the limb appear as a cone shape with a radial propagation and a constant angular width (Webb *et al.*, 1997). From these observations, several authors have proposed cone models to estimate the 3D parameters of HCMEs (*e.g.* Howard *et al.*, 1982; Fisher and Munro, 1984; Leblanc *et al.*, 2001; Zhao, Plunkett, and Liu, 2002; Michalek, Gopalswamy, and Yashiro, 2003; Xie, Ofman, and Lawrence, 2004; Xue, Wang, and Dou, 2005; Michalek, 2006).

Zhao, Plunkett, and Liu (2002) developed a cone model based on the coordinate transformation between the heliocentric coordinate system and the cone coordinate system. In this model, the parameters are determined with a visual fitting method until the modeled halo fits the observed CME halo. Xie, Ofman, and Lawrence (2004) proposed an analytical method using the relation of the cone and its elliptical projection (we call this model the elliptical-cone model here) to achieve unambiguous results and save on computational time. Xue, Wang, and Dou (2005) presented an ice-cream-cone model assuming that the structure of the CME resembles a symmetrical ice-cream cone, combining a cone with a sphere. This model can be applied to both halo CMEs and normal CMEs. Michalek (2006) reported an asymmetric-cone model, assuming that the structure of the CME is a cone with an elliptical cross section.

These models don't have been compared in great depth. In this study, we consider three cone models: the elliptical-cone model, the ice-cream-cone model, and the asymmetric-cone model. We apply these models to 62 HCMEs observed in the years 2001 to 2002. Then we compare the model parameters (*e.g.* the radial velocity, angular width, and source location). The article is organized as follows: Section 2 describes the data and the cone models, Section 3 presents the results obtained from these models, and the discussion. A brief summary and conclusion are given in Section 4.

2. Data and Method

We used frontside full HCMEs in the SOHO/LASCO CME catalog (//cdaw.gsfc.nasa.gov/CME_list/) from 2001 to 2002. During this period, 75 frontside full HCMEs were recorded out of 115 full HCMEs. Because 13 events are only observed in the C2 field of view or are too faint to measure their projection speeds, we selected 62 well-observed HCMEs. Figure 1 shows one of these HCMEs.

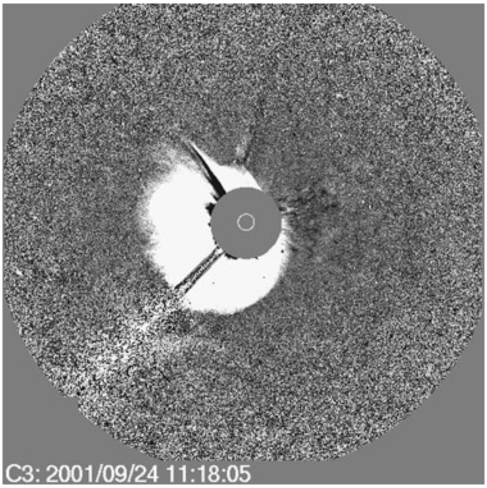

Figure 1 The halo CME observed by LASCO C3 coronagraph at 11:18 UT, on 24 September 2001.

We considered three cone models with the coordinate transformation between the heliocentric coordinate system [x_h, y_h, z_h] and the cone coordinate system [x_c, y_c, z_c]. These models have the same four assumptions: i) the structure of the CME is a cone, ii) the apex of the cone is located at the center of the Sun, iii) the propagation of the CME is radial, and iv) the radial velocity and the angular width are nearly constant.

Using these models, we can obtain the parameters describing the HCMEs: the radial velocity [V], the angular width [α in Figure 2], the source location [colatitude θ, and longitude ϕ in Figure 2], and the angle between the plane of the sky and the central axis of the cone [γ in Figure 2, $\sin\gamma = \sin\theta\cos\phi$].

To obtain the model parameters, we first measured the projection speeds of the CMEs by using the running-difference images of the LASCO-C3 observation. For this, we recorded the front edges of the CME on different azimuthal angles (every 15°, 24 points) at a given time. Then the projection speeds were estimated from a linear fitting between time and height.

2.1. Elliptical Cone Model

The elliptical-cone model (Xie, Ofman, and Lawrence, 2004) is an extension of the cone model developed by Zhao, Plunkett, and Liu (2002). This model considers that the shape of the CMEs is a symmetrical circular cone, the projection of which is an ellipse. Figure 2(a) shows the structure of the elliptical-cone model. The x_h-axis points to the Earth and the y_h–z_h plane defines the sky plane. The z_c-axis is the cone axis, and the x_c–y_c plane is parallel to the base of the cone. The cone axis is defined by the longitude angle ϕ, the colatitude angle θ, and the angular width of the cone α. To obtain the parameters of a HCME, first the model determines the CME angular width and source location [colatitude θ, longitude ϕ] using the geometric parameters of the elliptic projection such as major and minor axes,

$$\sin\gamma = \frac{a}{b}, \tag{1}$$

$$\tan\frac{\alpha}{2} = \frac{b}{h}\cos\gamma, \tag{2}$$

$$\tan\frac{\pi}{2} - \theta = \frac{\cos\gamma \sin\epsilon}{((\cos\gamma\cos\epsilon)^2 + (\sin\gamma)^2)^{\frac{1}{2}}} \tag{3}$$

$$\tan\phi = \frac{\cos\gamma\cos\epsilon}{\sin\gamma}, \tag{4}$$

where a is the semi-minor radius, b is the semi-major radius, h is the distance of the center of the elliptic projection from the center of the Sun, ϵ is the angle between the projection of the cone axis and y_h-axis, and γ is the angle between cone axis [z_c] and the plane of the sky [y_h–z_h plane]. Then the radial velocities are estimated with Equations (10) – (13) by Xie, Ofman, and Lawrence (2004) from the projection speeds measured at different position angles.

2.2. Ice-Cream-Cone Model

The ice-cream-cone model (Xue, Wang, and Dou, 2005) assumes that the shape of CMEs is a symmetrical ice-cream cone, combining a cone with sphere. The structure of the ice-cream cone is described in Figure 2(b). The x_h-axis points to the Earth and the y_h–z_h plane defines the plane of the sky. The z_c-axis is the cone axis, and the x_c–y_c plane is parallel to the base of the cone. θ and ϕ are the colatitude and longitude, and α is the angular width. This model considers three steps to determine the parameters. First, the possible source location of a HCME is restricted to a region near the flare location or active region. Second, the projection speeds measured at different position angles are determined by using the linear fitting method between height and time. Finally, we find the best-fit parameters by using the least-squares fitting method of the measured projected speeds and the estimated projected speeds using the following equations:

$$V_p = V\cos\delta, \tag{5}$$

$$\sin\delta = \frac{\cos\frac{\alpha}{2}\cos\phi\sin\theta \pm A\sqrt{\cos^2\phi\sin^2\theta + A^2 - \cos^2\frac{\alpha}{2}}}{\cos^2\phi\sin^2\theta + A^2}, \tag{6}$$

$$A = \cos\psi\sin\phi\sin\theta + \sin\psi\cos\theta, \tag{7}$$

where V_p is the projection speed, V is the radial velocity, δ is the angle between an arbitrary generatrix on the cone surface and the plane of the sky, and ψ is the azimuthal angle of a cone generatrix's projection in the plane of the sky.

2.3. Asymmetric Cone Model

The asymmetric-cone model (Michalek, 2006) assumes that the shape of an HCME is an asymmetric cone and its cross section is an ellipse. Figure 2(c) shows the structure of the asymmetric cone. The x_h-axis points to the Earth, and the y_h–z_h plane defines the plane of the sky. The z_c-axis is the cone axis, and the x_c–y_c plane is parallel to the base of the cone. θ and ϕ are the colatitude and longitude, and α is the angular width. This model determines the cone-model parameters on the basis of the following process. First, using the linear fit method between height and time, the projection speeds at the different position angles are determined. Second, the parameters are obtained by using numerical simulation through minimizing the root-mean-square [RMS] error between the measured projected speeds and the estimated projected speeds. In this step, the Equation (5) – (7) of Section 2.2 is also used. This model estimates the different angular widths at the different position angles (24 points) due to the elliptic cross section. The highest value of the angular widths [α in Figure 2(c)] is used to compare with those from the other cone models.

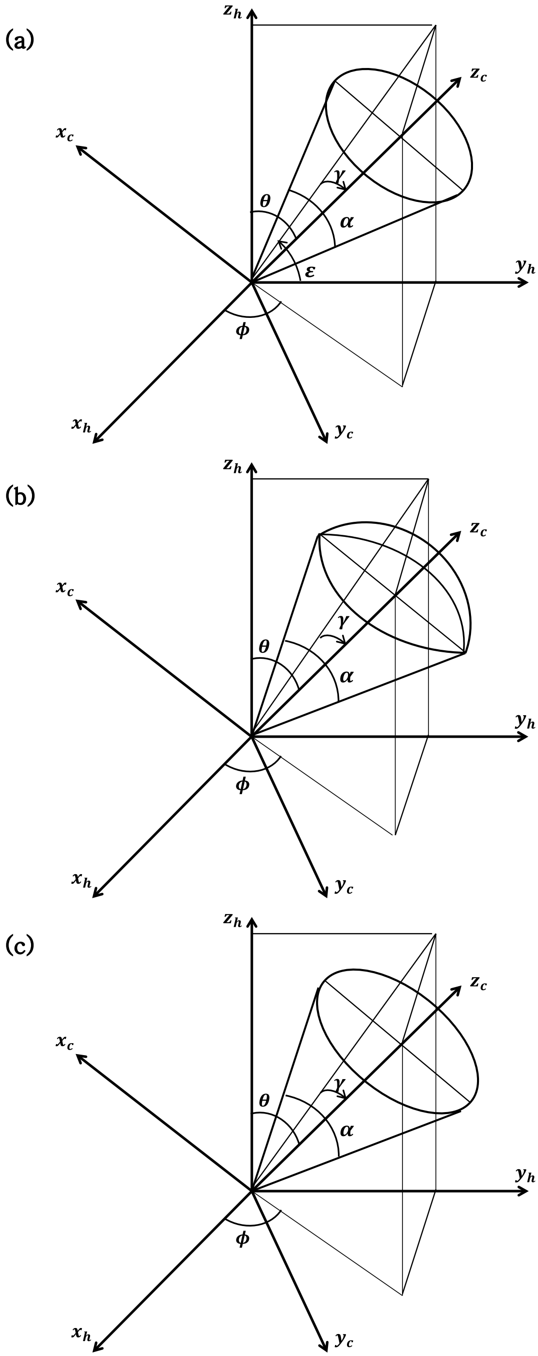

Figure 2 The structure of the cone models and the relationship between the heliocentric coordinate system (x_{h}, y_{h}, z_{h}) and the cone coordinate system (x_{c}, y_{c}, z_{c}). (a) is the elliptical-cone model (Xie, Ofman, and Lawrence, 2004), (b) is the ice-cream-cone model (Xue, Wang, and Dou, 2005), and (c) is the asymmetric-cone model (Michalek, 2006).

3. Results and Discussion

We determined the cone-model parameters of HCMEs for three cone models and compared the parameters for the following three pairs: (a) the elliptical-cone model and the ice-cream-cone model, (b) the elliptical-cone model and the asymmetric cone model, and (c) the ice-cream-cone model and the asymmetric-cone model.

Figures 3(a)–(c) show the comparison of the radial velocities for the three pairs mentioned above. Correlation coefficients of the radial velocities are CC = 0.80 for pair (a), CC = 0.82 for pair (b), and CC = 0.86 for pair (c). The radial velocities determined from these models are well correlated.

It is not possible to confirm whether the radial velocities obtained from the models are similar to the observations, as we do not know the actual radial velocity because of the projection effect. Therefore we compared the measured projected speeds obtained from the observations with the estimated projected speeds determined from the models. Figure 4(a)–(c) presents the comparison of the highest measured project speeds with their project speeds obtained from the three cone models. The correlation coefficients are CC = 0.71 for the elliptical-cone model, CC = 0.94 for the ice-cream-cone model, and CC = 0.94 for the asymmetric-cone model. We also calculated the mean absolute errors and the RMS errors between the highest values. The mean absolute error and the RMS error of the asymmetric-cone model (117 $\mathrm{km\,s^{-1}}$ and 152 $\mathrm{km\,s^{-1}}$) are smaller than other models (the elliptical-cone model: 297 $\mathrm{km\,s^{-1}}$ and 376 $\mathrm{km\,s^{-1}}$, the ice-cream-cone model: 138 $\mathrm{km\,s^{-1}}$ and 169 $\mathrm{km\,s^{-1}}$). As a result, the asymmetric-cone model has smaller errors than the other models. However, we cannot state that the asymmetric-cone model is better than the other models, because the methods for estimating the radial velocities are different from each other.

Figures 5(a)–(c) present the comparison of the angular widths for the same pairs. The correlation coefficients of the angular widths are CC = 0.10 for pair (a), CC = 0.27 for pair (b), and CC = 0.48 for pair (c). The average angular widths are 108° for the elliptical-cone model, 88° for the ice-cream cone model, and 92° for the asymmetric-cone model. Figures 6(a)–(c) show the comparison of the γ-values for the same pairs. The correlation coefficients of the angle γ are CC = −0.08 for pair (a) and CC = 0.07 for pair (b). For pair (c), the correlation coefficient (CC = 0.47) is higher than that of the other two pairs. The correlation coefficients of the angular widths and the γ-values are much smaller than expected. The reason is probably the different assumptions of these models.

From Figure 6(a), we can find that the values of γ representing the source location of the elliptical-cone model are all below 80°. Accordingly, the source locations obtained from this model are not located near the center of the Sun ($\gamma \rightarrow \frac{\pi}{2}$). This model assumes that the projection of the cone is an ellipse. If the projection of the cone is a circle and the center of the projection is located at the center of the Sun ($a = b$, and $h = 0$, in Equations (1) and (2)), the solution is degenerate since the angular width is not unique. These cases occur when the cone axis is aligned with the line of sight ($\theta = \frac{\pi}{2}$ and $\phi = 0$, see Xie, Ofman, and Lawrence, 2004). Thus, the source locations of the elliptical-cone model have a tendency to avoid the center of the Sun to estimate the angular width with a unique solution. If the projection of the cone is a circle ($a = b$, in Equation (1)), we obtain $\cos\gamma = 0$. In this case ($\tan\frac{\alpha}{2} = 0$, in Equation (2)), the angular width α is 2π. This means that the structure of the CME is a sphere.

In our results, the correlation coefficients of the angular widths and the values of γ between the ice-cream-cone model and the asymmetric-cone model are larger than others. A possible reason is that these models use the same relation between the projection speed and the radial speed (Equation (5) and Equation (6)) to estimate the parameters. Nevertheless,

Table 1 Characteristics of the models.

	Formula	Characteristic
Elliptical-cone model (symmetrical cone)	$\sin\gamma = \frac{a}{b}$ $\tan\frac{\alpha}{2} \propto \cos\gamma$ $\tan\frac{\pi}{2} - \theta$ and $\tan\phi \propto \cos\gamma$	$a \sim b$ $\sin\gamma \to 1 \therefore \cos\gamma \to 0$ $\theta \to \frac{\pi}{2}, \phi \to 0, \alpha = 0$ or 2π $\Rightarrow \alpha$ may not be reasonable when $a \approx b$
Ice-cream-cone model (symmetrical cone)	Equation (6) $\cos\frac{\alpha}{2} \leq \sin\theta\cos\phi$ $\gamma \to \frac{\pi}{2} \Rightarrow 0 \leq \alpha \leq \pi$ $\gamma \to 0 \Rightarrow \alpha \to \frac{\pi}{2}$	α: only one value $\Rightarrow \gamma$ has fewer constraints than the asymmetric cone model
Asymmetric cone model (asymmetric cone)	$\alpha \to \pi \Rightarrow \frac{\pi}{2} - \frac{\alpha}{2} \leq \gamma \leq \frac{\pi}{2}$ $\alpha \to 0 \Rightarrow \gamma \to \frac{\pi}{2}$	α : 24 values $\Rightarrow$ all values have to satisfy the condition $\Rightarrow$ as α_{min} decreases, γ increases γ may be overestimated

the angular width and the angle γ of these models are quite different because of their different assumptions.

Equation (6), estimating the parameters in the ice-cream-cone model and the asymmetric-cone model, has a real root for any position angle, if $\cos\frac{\alpha}{2} \leq \sin\theta\cos\phi = \sin\gamma$ (Xue, Wang, and Dou, 2005). If $\gamma \to \frac{\alpha}{2}$ (the source location is close to the Sun), the angular width [α] has any value between 0 and π to satisfy the above condition. As $\gamma \to 0$ (the source location is close to the limb), the angular width α approaches π. As $\alpha \to \pi$, the angle γ has any value between $\frac{\pi}{2} - \frac{\alpha}{2}$ and $\frac{\pi}{2}$, and if $\alpha \to 0$, the angle γ has a value close to $\frac{\alpha}{2}$.

From Figure 6(c), we can find that the values of γ of the asymmetric cone model are all higher than 60°. This means that the source locations obtained from the asymmetric cone model are located near the center of the Sun. The asymmetric-cone model assumes that the structure of a CME is an elliptical cone. Thus the angular widths measured at different position angles have different values. To obtain the real roots from the Equation (6), all angular widths have to satisfy the above condition. Since the minimum angular width, which may be small, satisfies the condition, angle γ has a higher value. On the other hand, the ice-cream-cone model assumes that the structure of a CME is a circular cone with a sphere. Therefore the angular width of this model is only a value that provides a much lower constraint of γ than that of the asymmetric cone model. Consequently, this model has a wide range of γ (30° – 90°) as shown in Figure 6.

It is well known that major CMEs are associated with flares. If a CME is radially ejected near the flare site, we expect that both locations are similar to each other. To confirm this, we compared the longitude estimated from the models with the longitude of the flare locations. Figures 7(a) – (c) show the relationship between the longitudes from the flare locations and those from the cone models. The correlation coefficients of the three cone models are CC = 0.45 for the elliptical-cone model, 4 CC = 0.76 for the ice-cream-cone model, and CC = 0.77 for the asymmetric-cone model. For all models, the estimated longitudes agree to within 50 degrees, which may be due to our selection of full halo CMEs. The longitudes of the ice-cream-cone and asymmetric-cone models are more inclined to the solar-disk center than those of the associated flares, which seems to be explained by the characteristics of γ and angular widths that are discussed above (for a summary see Table 1). The longitudes of the elliptical-cone model are somewhat scattered, which may be caused by the solution of its source location, which avoids the solar center.

Table 2 Parameters obtained by the three cone models during 2001 – 2002.

CME Catalog				Elliptical-cone model				Ice-cream-cone model				Asymmetric-cone model			
Date	Time	V	Flare	Velocity	α	Location	γ	Velocity	α	Location	γ	Velocity	α	Location	γ
10 Jan 01	00:54	832	N13E36	716	148	S32E25	49	850	86	S05E20	69	990	75	S04E15	74
20 Jan 01	19:31	839	S07E40	930	84	N13E01	76	800	160	S25E44	41	780	132	S00E15	75
20 Jan 01	20:30	1507	S07E46	1585	125	N08E28	61	1600	76	N09E14	73	1450	91	N09E15	73
28 Jan 01	15:54	916	S04W59	764	119	N34W19	52	1001	132	S22W49	37	1160	91	S12W20	67
10 Feb 01	05:54	956	N37W03	1243	84	S24W18	60	1220	42	N14E03	76	980	64	N14E04	75
11 Feb 01	01:31	1183	N24W57	1708	73	N34W13	71	1130	80	N13W14	71	1020	91	N15W14	70
19 Mar 01	05:26	389	S20W00	728	146	S04E33	57	780	92	N09E04	80	760	100	S08E01	82
24 Mar 01	20:50	906	N15E22	592	161	N31E09	67	680	170	N39E17	48	680	167	N04E12	77
25 Mar 01	17:06	677	N16E25	1306	118	N04E25	65	1110	91	S07E04	82	1010	95	S07E04	82
28 Mar 01	12:50	519	S10E30	840	81	S23E01	67	620	136	N13E12	72	750	94	N08E07	79
29 Mar 01	10:26	942	N20W19	1336	161	N01E33	57	860	152	N35W18	51	870	155	S15E17	67
01 Apr 01	11:26	1475	S22E90	1644	100	S13E32	56	1980	54	S07E22	67	1710	58	S04E14	75
05 Apr 01	17:06	1390	S24E50	1485	120	N29W03	61	1230	118	N08E31	58	1580	79	N04E15	74
06 Apr 01	19:30	1270	S21E31	1103	123	S31E21	53	1320	78	S04E02	86	900	155	S14E09	73
09 Apr 01	15:54	1192	S21W04	1460	102	S28E10	60	1030	128	S21W29	55	1410	81	S09W11	76
10 Apr 01	05:30	2411	S23W09	2102	131	S24W09	64	1880	92	S11W13	73	2740	62	S06W07	81
11 Apr 01	13:31	1103	S22W27	1426	101	S23W21	59	1590	48	S02W02	87	770	134	S09W08	78
12 Apr 01	10:31	1184	S19W43	1679	110	S26W27	53	1810	48	S02W08	82	1740	80	S05W12	77
26 Apr 01	12:30	1006	N23W02	1153	130	N06W37	52	1920	46	N04E08	81	1670	60	N05E09	80
14 Aug 01	16:01	618	N16W36	829	131	N26E24	55	790	74	N09W00	81	690	116	N12E09	75
25 Aug 01	16:50	1433	S17E34	1845	65	S14E08	74	1860	97	S18E12	68	1850	99	S18E12	68

Table 2 (*Continued*)

CME Catalog				Elliptical-cone model				Ice-cream-cone model				Asymmetric-cone model			
Date	Time	V	Flare	Velocity	α	Location	γ	Velocity	α	Location	γ	Velocity	α	Location	γ
11 Sep 01	14:54	791	N13E35	979	161	S18W45	42	650	81	N02E14	76	620	94	N04E14	75
24 Sep 01	10:30	2402	S16E23	2501	70	N16E08	73	2020	108	S17E36	51	2830	60	S08E16	72
28 Sep 01	08:45	846	N12E18	1392	112	N23W22	58	1130	72	N10W00	80	1150	79	S10W00	80
01 Oct 01	05:30	1405	S24W81	1130	80	S24W14	62	1410	88	S20W20	62	1510	62	S11W12	74
09 Oct 01	11:30	973	S30E10	1202	97	S07W21	68	1080	107	S33E04	57	1126	91	S15E02	75
19 Oct 01	01:27	558	N16W18	1420	141	N24E21	58	1270	36	N02W07	83	1180	45	N02W07	83
19 Oct 01	16:50	901	N15W29	941	144	N28E24	54	1400	69	N06E03	83	1080	108	N10E05	79
22 Oct 01	15:06	1336	S21E18	1727	115	S26E28	52	1600	62	S08E11	76	1740	58	S07E10	78
25 Oct 01	15:26	1092	S18W20	1449	102	S24W07	65	1470	64	S08W02	82	1070	110	S15W03	75
01 Nov 01	22:30	453	N12W23	456	131	N20E14	66	450	134	N01W26	64	460	177	N08W22	67
03 Nov 01	19:20	457	N04W20	712	108	N30W01	60	660	81	N13W11	73	710	81	N12W10	74
04 Nov 01	16:35	1810	N06W18	2757	150	S24W24	57	2870	70	S03W05	84	2820	81	S03W05	84
17 Nov 01	05:30	1379	S13E42	1465	117	N29W22	54	1220	118	N18E24	60	1530	86	N11E12	74
21 Nov 01	14:06	518	S14W19	1035	155	S29E10	60	890	78	S08E01	82	660	132	N19W04	71
22 Nov 01	20:30	1443	S25W67	2185	81	S16W23	62	1970	49	S06W11	77	1630	60	S07W14	74
22 Nov 01	23:30	1437	S17W36	1501	110	N09W21	67	1540	122	N01W24	66	1860	99	N02W14	76
28 Nov 01	17:30	500	N04E16	976	165	N20E39	47	540	89	N01W07	83	410	175	S09W15	73
13 Dec 01	14:54	864	N16E09	1591	48	N08E08	79	1110	68	N04W01	86	690	166	N15E01	75
14 Dec 01	09:06	1506	N07E86	1404	70	N04E20	69	1450	87	N16E13	69	1400	90	N14E15	70
28 Dec 01	20:30	2216	S24E90	2309	87	S24W15	62	1640	111	S24E33	50	2870	50	S08E10	77
04 Jan 02	09:30	896	N38E87	1552	58	S05E15	74	1480	64	N06E03	83	1400	80	N07E03	82

Table 2 (*Continued*)

CME Catalog				Elliptical-cone model				Ice-cream-cone model				Asymmetric-cone model			
Date	Time	V	Flare	Velocity	α	Location	γ	Velocity	α	Location	γ	Velocity	α	Location	γ
14 Jan 02	05:35	1492	S28W90	1707	111	N30W22	54	1600	110	S15W30	57	1720	96	S10W20	68
20 Feb 02	06:30	952	N12W72	905	106	N19E12	68	1020	56	S01W10	80	1270	47	S01W08	82
10 Mar 02	23:06	1429	S22E90	1416	89	S16E23	62	1400	114	S10E24	64	1300	125	S07E17	72
11 Mar 02	23:30	950	S15E45	1138	75	N20E09	68	1020	85	S11E13	73	1520	54	S06E07	81
14 Mar 02	17:06	907	S23E57	939	128	S43E17	44	1100	172	S00E49	41	1400	102	S12E04	77
15 Mar 02	23:06	957	S07W08	758	146	N18W14	67	770	132	N22E04	68	790	143	N18W01	72
18 Mar 02	02:54	989	S10W30	706	164	N32W20	53	1350	64	N02W04	84	1290	73	N02W07	83
22 Mar 02	11:06	1750	S10W90	1086	96	S11W35	54	1760	62	S08W19	69	1300	76	S09W25	64
15 Apr 02	03:50	720	S15W01	624	161	S05W15	75	960	84	N04E01	86	1130	76	N03W00	87
17 Apr 02	08:26	1240	S13W12	1834	56	N03W11	79	1790	56	S05W11	78	1780	57	N05W11	78
21 Apr 02	01:27	2393	S14W84	2166	74	S03W25	65	2700	62	S00W20	70	2700	62	N04W16	71
22 May 02	03:26	1557	S15W70	1806	59	S12W14	72	1710	74	S10W10	76	1780	88	S10W09	77
15 Jul 02	20:30	1151	N19W01	1585	85	N20E16	65	1100	83	N14E14	70	1100	87	N11E10	74
26 Jul 02	22:06	818	S19E26	1375	86	N22W10	66	830	106	S29E20	55	1120	64	S13E10	74
16 Aug 02	12:30	1585	S10E19	1764	76	S15E09	73	1300	128	S36E13	52	1700	83	S13E05	76
22 Aug 02	02:06	998	S07W62	1516	97	S21W21	61	1280	65	S10W10	76	1400	66	S07W08	79
24 Aug 02	01:27	1913	S02W81	2149	102	S12W35	53	2970	42	S03W13	77	2880	50	S03W11	79
09 Nov 02	13:31	1838	S19W29	2280	92	S28W31	49	2570	40	S08W09	78	2920	44	S08W06	81
24 Nov 02	20:30	1077	N20E35	1546	62	N16E02	74	930	132	N16E14	69	1090	113	N12E04	77
19 Dec 02	22:06	1092	N15W09	1017	139	N12W33	55	1380	60	N03W13	77	1230	64	N03W13	77

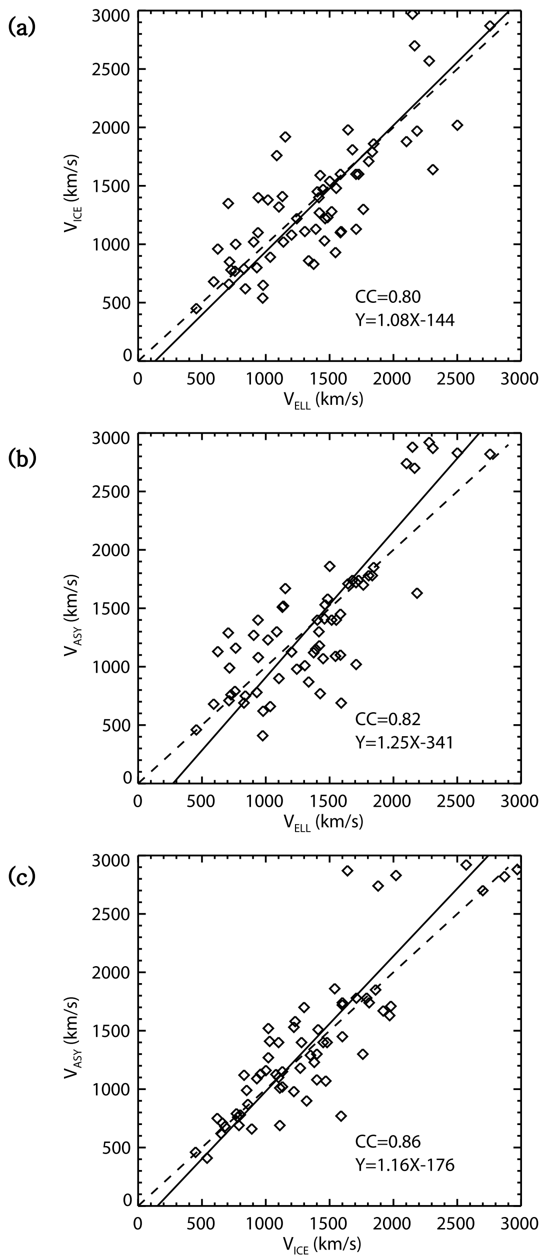

Figure 3 Comparison of the radial velocities from the three cone models. Diamond symbols represent the results obtained from the models, the solid line is a linear fit to all data points, and the dashed line is a diagonal line with a slope of one.

The cone-model parameters of the 62 HCMEs from this study are summarized in Table 2. The first four columns give the information of each CME: date, time of first appearance in the LASCO field of view, apparent speed from the SOHO/LASCO catalog, and flare location from the NOAA/NGDC. Columns 5 – 8 are the radial velocity, the angular width, the source

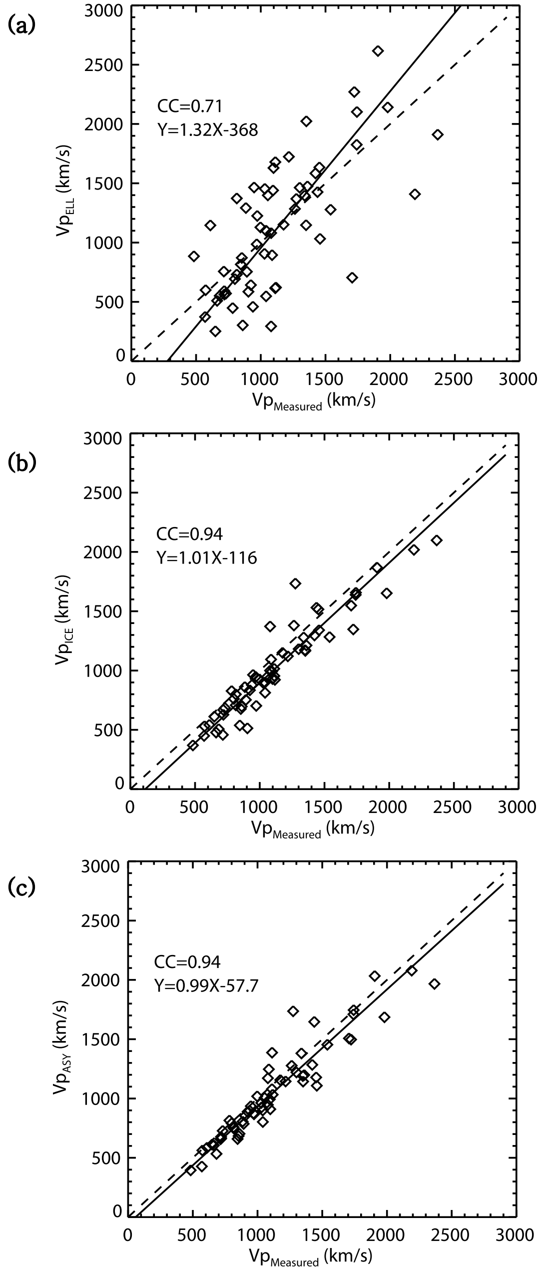

Figure 4 Comparison of the highest values of the measured projection speeds and the estimated projection speeds from the cone models. Diamond symbols represent the estimated values in terms of the measured values, the solid line is a linear fit to all data points, and the dashed line is a diagonal line with a slope of one.

location, and the angle [γ] obtained by the elliptical cone-model. Columns 9 – 12 and 13 – 16 are the same parameters derived from the ice-cream-cone model and the asymmetric-cone model, respectively.

Figure 5 Comparison of the angular widths from the three cone models. Diamond symbols represent the results obtained from the models, the solid line is a linear fit to all data points, and the dashed line is a diagonal line with a slope of one.

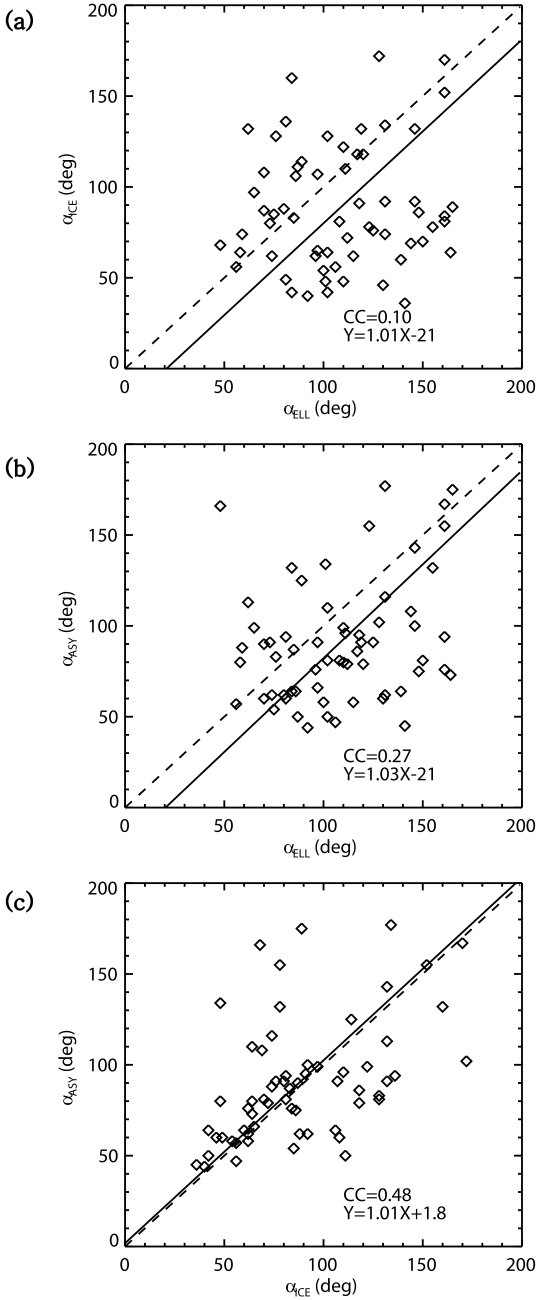

4. Summary and Conclusion

To forecast geomagnetic storms, it is important to determine the kinematic and geometric parameters of HCMEs (*e.g.* the radial velocity, the angular width, and the angle γ). We

Figure 6 Comparison of the angle between the cone axis and the plane of the sky from the three cone models. Diamond symbols represent the results obtained from the models, and the dashed line is a diagonal line with a slope of one.

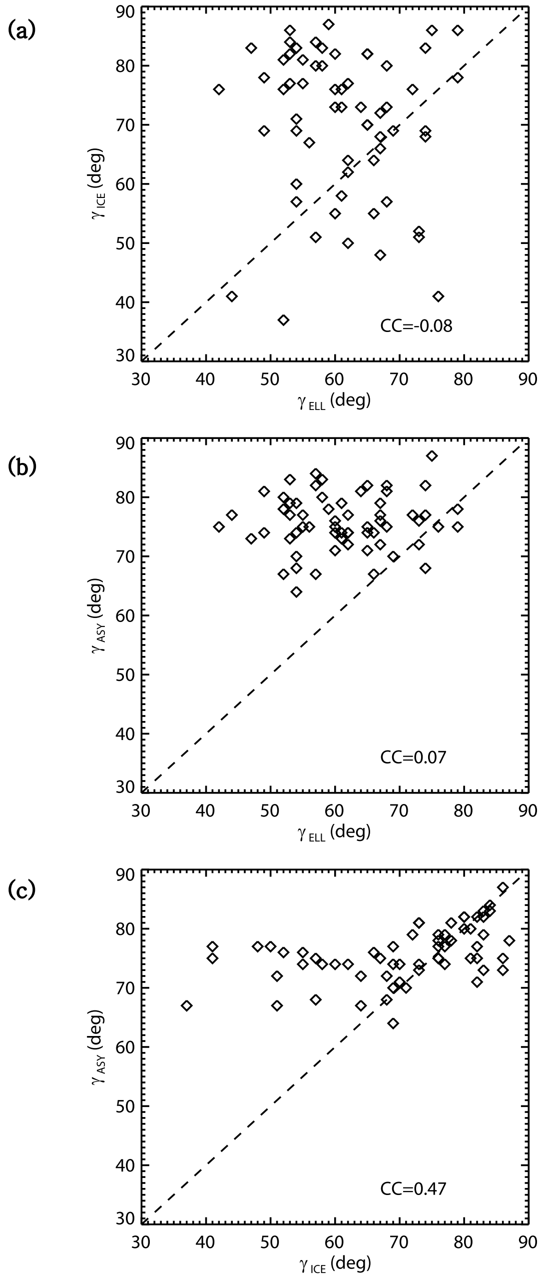

considered three cone models (elliptical-cone model, ice-cream-cone model, asymmetric-cone model).

The results show that the radial velocities determined from the cone models are well correlated with one another. The reason is that these models used the same projection speeds to estimate the radial velocity.

Figure 7 Comparison of the longitudes of the flare location and those of the source location estimated from the cone models. Diamond symbols represent the estimated values in terms of the observed values, the solid line is a linear fit to all data points, and the dashed line is a diagonal line with a slope of one.

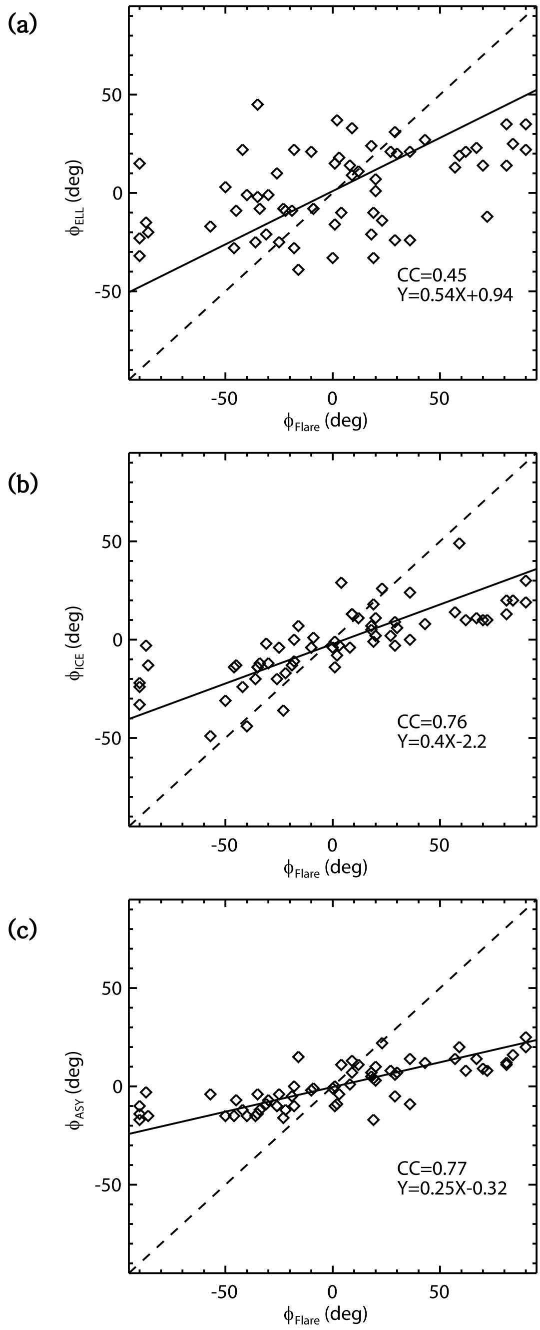

The results of the angular width and the angle γ are somewhat different. The reason is probably the different assumptions of these models for the structure of a CME. The elliptical-cone model assumes a circular cone and an elliptical projection, the ice-cream-cone model assumes a circular cone with a spherical top, and the asymmetric-cone model assumes an asymmetric cone with an elliptic cross section (see Table 1).

Strengths and weaknesses of the three models from this study can be summarized in terms of space weather application as follows. For the source location, the results of the elliptical cone model are not located near the solar center. The asymmetric-cone model tends to estimate the source location to be near the center. For the angular width, the elliptical-cone model tends to estimate larger values than those of other two models. For the radial velocity, the results of the three cone models are similar to each another. The ice-cream-cone model has the advantage that it can be applied to partial-halo CMEs (Kim *et al.*, 2013).

According to our results, the radial velocities obtained from the cone models can be applied to space-weather forecast. For example, the WSA/ENLIL cone model (Taktakishvili *et al.*, 2009; Falkenberg *et al.*, 2010; Taktakishvili, MacNeice, and Odstrcil, 2010) requires input parameters from a cone model. The values of the angular width are only poorly correlated. Therefore it is still necessary to study the parameters.

Acknowledgements This work has been supported by the WCU program (No. R31-10016) through the National Research Foundation of Korea funded by the Ministry of Education, Science and Technology and by the Korea Research Foundation Grant funded by the Korean Government (MOEHRD, Basic Research Promotion Fund) (20090071744 and 20100014501), and the Korea Meteorological Administration/National Meteorological Satellite Center. SOHO is a mission of international cooperation between ESA and NASA. We acknowledge the use of data from the LASCO CME catalog. The CME catalog is generated and maintained by the Center for Solar Physics and Space Weather, Catholic University of America, in cooperation with the Naval Research Laboratory and NASA.

References

Brueckner, G.E., Howard, R.A., Koomen, M.J., Korendyk, C.M., Michels, D.J., Moses, J.D., *et al.*: 1995, The Large Angle Spectroscopic Coronagraph (LASCO). *Solar Phys.* **162**, 357. doi:10.1007/BF00733434.

Brueckner, G.E., Delaboudinière, J.P., Howard, R.A., Paswaters, S.E., St. Cyr, O.C., Schwenn, R., *et al.*: 1998, Geomagnetic storms caused by coronal mass ejections (CMEs): March 1996 through June 1997. *Geophys. Res. Lett.* **25**, 3019. 1996, through, June, 1997.

Cane, H.V., Richardson, I.G., St. Cyr, O.C.: 2000, Coronal mass ejections, interplanetary ejecta and geomagnetic storms. *Geophys. Res. Lett.* **27**, 3591.

Falkenberg, T.V., Vršnak, B., Taktakishvili, A., Odstrcil, D., MacNeice, P., Hesse, M.: 2010, Investigations of the sensitivity of a coronal mass ejection model (ENLIL) to solar input parameters. *Space Weather* **8**, S06004.

Fisher, R.R., Munro, R.H.: 1984, Coronal transient geometry. I – the flare-associated event of 1981 March 25. *Astrophys. J.* **280**, 428.

Gopalswamy, N., Lara, A., Lepping, R.P., Kaiser, M.L., Berdichevsky, D., St. Cyr, O.C.: 2000, Interplanetary acceleration of coronal mass ejections. *Geophys. Res. Lett.* **27**, 145.

Gosling, J.T., McComas, J.D., Phillips, J.L., Bame, S.J.: 1991, Geomagnetic activity associated with Earth passage of interplanetary shock disturbances and coronal mass ejections. *J. Geophys. Res.* **96**, 9831.

Howard, R.A., Michels, D.J., Sheeley, N.R., Koomen, M.N.: 1982, The observation of a coronal transient directed at Earth. *Astrophys. J.* **263**, 101.

Kim, T.-H., Moon, Y.-J., Na, H., Lee, K.-S., Park, J.: 2013, Comparison of radial velocities of halo CMEs based on the GCS flux rope Model and an Ice Cream Cone Model. *Solar Phys.*, submitted.

Leblanc, Y., Dulk, G.A., Vourlidas, A., Bougeret, J.-L.: 2001, Tracing shock waves from the corona to 1 AU: type II radio emission and relationship with CMEs. *J. Geophys. Res.* **106**, 25301.

Michakel, G.: 2006, An asymmetric cone model for halo coronal mass ejections. *Solar Phys.* **237**, 101. doi:10.1007/s11207-006-0075-8.

Michakel, G., Gopalswamy, N., Yashiro, S.: 2003, A new method for estimating widths, velocities, and source location of halo coronal mass ejections. *Astrophys. J.* **584**, 472.

Taktakishvili, A., MacNeice, P., Odstrcil, D.: 2010, Model uncertainties in predictions of arrival of coronal mass ejections at Earth orbit. *Space Weather* **8**, S06007.

Taktakishvili, A., Kuznetsova, M., MacNeice, P., Hesse, M., Rastatter, L., Pulkkinen, A., *et al.*: 2009, Validation of the coronal mass ejection predictions at the Earth orbit estimated by ENLIL heliosphere cone model. *Space Weather* **7**, S03004.

Wang, Y.M., Yee, P.Z., Wang, S., Zhou, G.P., Wang, J.X.: 2002, A statistical study on the geoeffectiveness of Earth-directed coronal mass ejections from March 1997 to December 2000. *J. Geophys. Res.* **107**(A11), 1340.

Webb, D.F., Kahler, S.W., McIntosh, P.S., Klimchuck, J.A.: 1997, Large-scale structures and multiple neutral lines associated with coronal mass ejections. *J. Geophys. Res.* **102**, 24161.

Webb, D.F., Cliver, R.W., Crooker, N.U., St. Cyr, O.C., Thompson, B.J.: 2000, Relationship of halo coronal mass ejections, magnetic clouds, and magnetic storms. *J. Geophys. Res.* **105**, 7491.

Xie, H., Ofman, L., Lawrence, G.: 2004, Cone model for halo CMEs: application to space weather forecasting. *J. Geophys. Res.* **109**, A03109.

Xue, X.H., Wang, C.B., Dou, X.K.: 2005, An ice-cream cone model for coronal mass ejections. *J. Geophys. Res.* **110**, A08103.

Zhao, X.P., Plunkett, S.P., Liu, W.: 2002, Determination of geometrical and kinematical properties of halo coronal mass ejections using the cone model. *J. Geophys. Res.* **107**(A8), SSH13.